Enhanced surface plasmon resonance imaging detection of DNA hybridization on periodic gold nanoposts

L. Malic,[1] B. Cui,[2] T. Veres,[2] and M. Tabrizian[1,*]

[1]*Biomedical Engineering Department, McGill University, Montreal, Quebec H3A 2T5, Canada*
[2]*Industrial Materials Institute, Boucherville, Quebec J4B 6Y4, Canada*
[*]*Corresponding author: maryam.tabrizian@mcgill.ca*

Received June 25, 2007; revised August 22, 2007; accepted August 29, 2007;
posted September 13, 2007 (Doc. ID 84405); published October 18, 2007

We explore periodic gold nanoposts as substrates for the enhanced surface plasmon resonance imaging (SPRi) detection of DNA hybridization. Rigorous coupled-wave analysis was used to model and design the nanopost-based SPRi biosensor. Arrayed gold nanoposts on gold-coated glass substrate, with various widths and periodicity, were fabricated using electron-beam lithography and characterized with scanning electron and atomic force microscopy. A scanning-angle SPRi apparatus was used to conduct the kinetic analysis of DNA hybridization on nanopost-based sensor surface and assess the corresponding SPR signal amplification. Experimental results showed that both the nanostructure size and period influenced the SPR signal enhancement; the optimized 30 nm height, 50 nm size, and 110 nm period nanoposts provided a fivefold SPR signal amplification compared with the plain 50 nm thick gold film used as control. © 2007 Optical Society of America

OCIS codes: 240.5420, 240.6680, 310.6860, 130.6010, 120.1880.

In the past decade, the surface-sensitive optical technique of surface plasmon resonance imaging (SPRi) has emerged as an attractive alternative to traditional fluorescence-based microarray detection methods for real-time, label-free detection of DNA hybridization. However, the sensitivity of SPRi is limited by a small angular shift of the SPR spectrum dip and a small fractional reflectivity change. To overcome the sensitivity limitation, nanoparticle-based SPR biosensors have drawn tremendous interest in recent years. The exploitation of nanoparticles allows strong optical coupling of incident light to plasmon resonances, so-called localized surface plasmons (LSPs). This phenomenon has given rise to a whole new host of biosensors based on localized SPR spectroscopy and has also been employed to enhance the signals of conventional SPR [1–4]. It has been empirically shown that colloidal gold (Au) nanoparticles attached to thin film of an SPR biosensor exhibit more than tenfold signal amplification [5]. The sensitivity enhancement is attributed to strong interactions between LSPs, SPs, and binding biomolecules in the presence of nanoparticles, leading to different resonance properties with an additional shift of resonance angle. However, while the nanoparticles generate pronounced SPR signals, they essentially transform an advantageous label-free sensing technique into a labeled one [6]. On the other hand, noble metal nanostructures fabricated on SPR active thin film can also be used to amplify the SPR signal. In comparison with colloidal Au nanoparticles, the use of periodic Au nanostructures provides the advantage of spatial uniformity and performance reproducibility, while retaining the benefit of SPR label-free detection. Recent theoretical studies have shown that the optimized design of periodic one-dimensional Au nanowires provides an order of magnitude sensitivity enhancement compared with conventional flat-surface SPR sensors [7–9]. In this context, periodic two-dimensional Au nanostructures should thus significantly improve the SPR signal response. However, unlike massive experimental research on SPR signal enhancement via conjugated Au nanoparticles, to our knowledge no experimental studies have been reported using periodic two-dimensional Au nanostructures. We demonstrate here both numerically and experimentally that periodic gold nanoposts fabricated on thin Au film can enhance the sensitivity of conventional SPRi. Experimental results indicate that both the nanostructure size and period play a role in SPR signal amplification.

The well-established rigorous coupled-wave analysis (RCWA) is successfully employed to corroborate the nanostructure size, period, and the initial Au film thickness to the experimental results [8,10]. A nanopost-based SPR biosensor is represented as an array of rectangular Au nanostructures residing on a gold thin film. The DNA hybridization event is modeled with a homogeneous single-stranded DNA (ssDNA) monolayer that changes its refractive index and thickness by 5% and 3.5 nm, respectively, to form a double-stranded DNA (dsDNA) [11]. The simulation is performed by scanning the incidence angle of a TM-polarized monochromatic plane wave at 800 nm wavelength with an angular resolution of 0.01°. The optimized nanostructures are selected based on the maximum shift of the SPR dip for the given refractive index change. The angular sensitivity enhancement factor ASEF is then defined as the ratio of resonant angle shift due to DNA hybridization on a nanostruc-

0146-9592/07/213092-3/$15.00

tured surface to that of a plain 50 nm thick gold film conventional SPR structure, used and referred to hereafter as the control:

$$\mathrm{ASEF} = \left| \frac{\Delta\Theta_{\mathrm{NSPR}}}{\Delta\Theta_{\mathrm{SPR}}} \right| = \left| \frac{\Theta_{\mathrm{NSPR(dsDNA)}} - \Theta_{\mathrm{NSPR(ssDNA)}}}{\Theta_{\mathrm{SPR(dsDNA)}} - \Theta_{\mathrm{SPR(ssDNA)}}} \right|,$$

where Θ_{NSPR} and Θ_{SPR} represent the resonant angle with and without the nanoposts, respectively [7]. To determine the optimum ratio of initial Au film thickness to that of nanopost height, the two parameters are changed from 0 to 60 nm and 10 to 100 nm, respectively, at a constant width and period. From the results obtained (not shown), the enhancement is observed for nanostructures not exceeding 40 nm in height for all Au film thicknesses, above which the control provides better sensitivity. Maximum angular shift is obtained for 30 nm high nanostructures residing on a 20 nm Au film. For optimization of nanostructure size and period, the two values were constant, while the nanopost width and spacing (periodicity) were varied from 30 to 100 nm and 30 to 170 nm, respectively (Fig. 1). The nanopost spacing that yields the highest ASEF is between 30 and 50 nm for differently sized nanostructures (Fig. 1). For instance, nanostructures that are 50 or 60 nm in size have maximum ASEF at a period that corresponds to 90 and 110 nm, respectively.

Following the simulation results, three substrates, each having four 400×400 μm arrays of differently sized nanostructures 30 nm in height with 80, 110, and 200 nm periods, are fabricated using electron beam lithography (EBL) on a 20 nm thick Au-coated SF-11 glass. Additionally, to investigate the effect of initial Au film thickness on the SPR response, two substrates with 30 nm high, 110 nm period nanoposts of various widths are fabricated on bare and 50 nm thick Au-coated SF-11 glass. Due to fabrication constraints, the nanostructure shape is simply defined by the shape of the beam, while the exposure dose is adjusted from 10 to 45 fC at 160 pA and 30 kV to obtain structures of different sizes. Figure 2(a) shows a sample scanning electron microscope (SEM) image of nanoposts of nominally circular shape with 110 nm period having a diameter of 50 ± 3.5 nm. Atomic force microscopy (AFM) characterization shows dome-shaped fabricated nanoposts [Fig. 2(b)], as expected

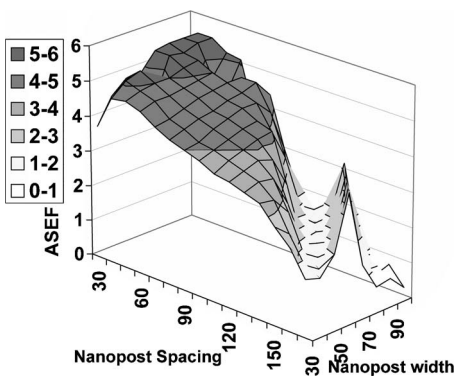

Fig. 1. Numerically obtained ASEF for SPR substrate with nanoposts of different size and periodicity.

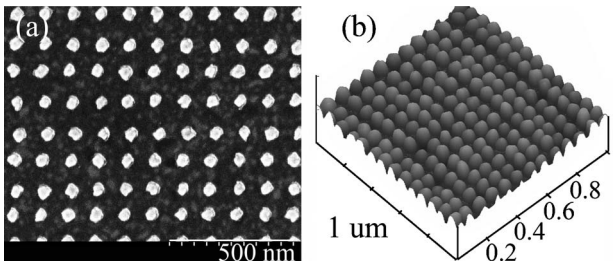

Fig. 2. Sample images of fabricated Au nanoposts 50 nm in size, 110 nm period (a) SEM image; (b) AFM surface plot.

from anisotropic gold evaporation in the narrow PMMA trenches defining the nanostructures. The height and the period of the nanoposts were found to be of excellent uniformity with 3.73% and 1.21% variation, respectively.

Surface functionalization of substrates is done using 1 μM thiol-modified 20 mer oligonucleotide probe sequence in 1 M KH_2PO_4 for 120 min. Following immobilization, substrates are treated with 1 mM mercaptohexanol for 90 min to render the probes highly accessible to the target while preventing unspecific target binding to the gold surface [12].

All DNA hybridization experiments are carried out using 20 mer oligonucleotide target sequence complementary to the immobilized probe. Hybridization kinetic curves are monitored using SPRi Lab+ apparatus equipped with 800 nm LED source and a CCD camera (Genoptique, France). A baseline signal is obtained first for hybridization buffer (1 M NaCl in TE buffer), followed by hybridization signal for which 250 nM target is injected into the flow cell, allowing the target to bind to the immobilized probe for 20 min to yield sufficient refractive index change (high hybridization efficiency) while keeping the reaction time low. Finally, the substrate is washed with buffer, and the difference in the reflected intensity is computed by the difference between the initial and final buffer injections. The kinetic curves of the reaction on the nanostructured surface are shown in Fig. 3 for (a) different initial gold film thickness, (b) nanopost period, and (c) nanopost size. To enable qualitative assessment of the effect of nanostructured surface for SPR signal amplification, similar to the ASEF, the reflectivity sensitivity enhancement factor RSEF $= \Delta R_{\mathrm{NSPR}} / \Delta R_{\mathrm{SPR}}$ (inset of Fig. 3) is included to describe the ratio of the change in reflected intensity due to DNA hybridization on the nanostructured surface (ΔR_{NSPR}), to that of the control (ΔR_{SPR}). The RSEF is important for real-time SPR sensing that relies on continuous monitoring of reflected light intensity at a specific angle, used in SPR imaging.

From the curves of Fig. 3(a), as the nanostructure size and period are kept constant at 50 and 110 nm respectively, the initial Au film thickness has little effect on the SPR signal amplification. However, in the absence of underlying SPR active thin Au film, the SPRi apparatus is almost incapable of tracking the kinetic changes of the reaction occurring on the nanostructured biosensor surface. For the optimum initial 20 nm thick Au film, the kinetic response for nanostructures 50 nm in size having 80, 110 and 200 nm

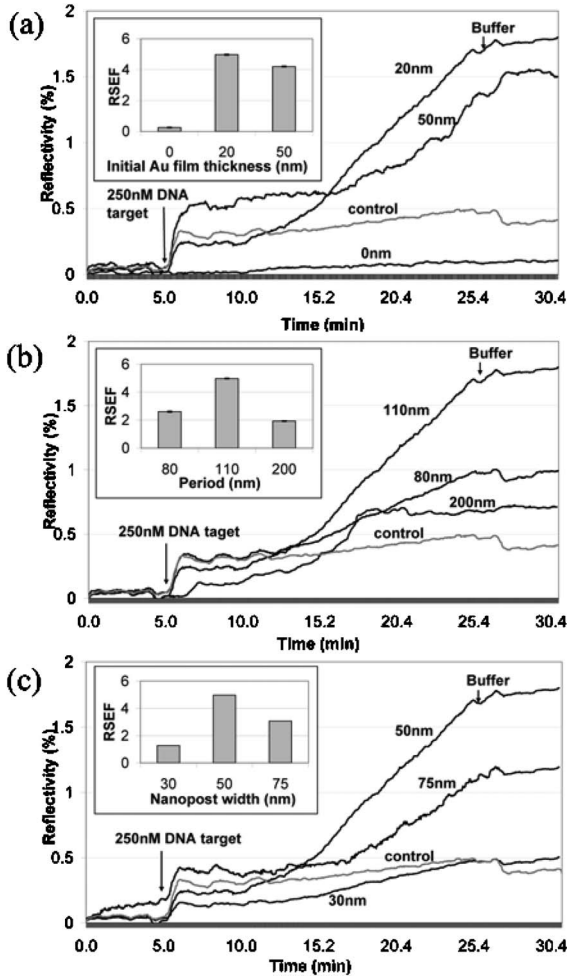

Fig. 3. Kinetic curves of 250 nM DNA target hybridization on nanostructured SPR substrate having nanoposts 30 nm in height with (a) 110 nm period, 50 nm width and different initial Au film thickness; (b) 50 nm width, underlying 20 nm thick Au film and different period; (c) 110 nm period, underlying 20 nm thick Au film and different size.

periods are shown in Fig. 3(b). From the curves it can be seen that the nanoposts having 80 and 110 nm periods exhibit higher reflectivity change compared with control than those with 200 nm period. The simulation predicted that smaller spacing between the neighboring structures allows for more pronounced coupling of localized and propagated surface plasmons in the presence of the dielectric layer resulting in enhanced electromagnetic fields. Although the periodicity plays the main role in the SPR signal amplification, the sensitivity enhancement can be further fine-tuned by nanostructure size. This is shown in Fig. 3(c), where nanoposts with 50 nm diameter and 110 nm period yield the highest signal amplification (RSEF=5), while the SPR response for 30 nm structures was comparable with the control. Similar size-dependent SPR signal results have been obtained for 80 and 200 nm period structures (results not shown). In particular, 50 nm wide nanoposts provided the highest signal amplification for all examined periods. However, it should be noted that for the same nanostructure size, the 110 nm period always provided superior performance. For instance, 75 nm size, the 110 nm period nanostructures amplified 2.5 $\times$ the signal, while the 200 nm period was inferior to the control. This is mostly due to weaker LSP–SPP coupling at larger nanopost spacing and more pronounced SPR curve broadening at larger nanostructure periods. These findings suggest that the fabrication process should be directed toward optimizing the period rather than the size of the nanostructures, given that the period is more easily controlled during EBL.

In this Letter, we have shown that a nanostructure-based SPR biosensor yields an enhancement in the sensitivity of conventional SPR imaging. We have demonstrated both numerically and experimentally that due to the increased surface binding area and the excitation and coupling of localized and bulk surface plasmons provided by the nanoposts, the SPR signal can be amplified up to five times in only 20 min, as was the case for 50 nm wide structures spaced 60 nm. This is significant sensitivity improvement in comparison with a conventional SPRi biosensor, with potential for future applications in rapid, ultrasensitive DNA detection and DNA microarray analysis.

The authors thank le Fonds québécois de la recherche sur la nature et les technologies (FQRNT) for the scholarship, FQRNT-team grant, FQRNT-Centre for Biorecognition and Biosensors, and the National Research Council of Canada for their financial support.

References

1. C. D. Chen, S. F. Cheng, L. K. Chau, and C. R. C. Wang, Biosens. Bioelectron. **22**, 926 (2007).
2. A. B. Dahlin, J. O. Tegenfeldt, and F. Hook, Anal. Chem. **78**, 4416 (2006).
3. A. J. Haes and R. P. Van Duyne, Anal. Bioanal. Chem. **379**, 920–930 (2004).
4. E. Hutter and J. H. Fendler, Adv. Mater. (Weinheim, Germany) **16**, 1685 (2004).
5. L. He, M. D. Musick, S. R. Nicewarner, F. G. Salinas, S. J. Benkovic, M. J. Natan, and C. D. Keating, J. Am. Chem. Soc. **122**, 9071 (2000).
6. S. J. Chen, F. C. Chien, G. Y. Lin, and K. C. Lee, Opt. Lett. **29**, 1390 (2004).
7. K. M. Byun, S. J. Kim, and D. Kim, Opt. Express **13**, 3737 (2005).
8. K. M. Byun, D. Kim, and S. J. Kim, Sens. Actuators B **117**, 401 (2006).
9. D. Kim, J. Opt. Soc. Am. A **23**, 2307 (2006).
10. S. Park, G. Lee, S. H. Song, C. H. Oh, and P. S. Kim, Opt. Lett. **28**, 1870 (2003).
11. S. Elhadj, G. Singh, and R. F. Saraf, Langmuir **20**, 5539 (2004).
12. A. W. Peterson, R. J. Heaton, and R. M. Georgiadis, Nucl. Acid Res. **29**, 5163 (2001).